Published in final edited form as:

Cancer Res. 2017 June 15; 77(12): 3217–3230. doi:10.1158/0008-5472.CAN-16-3304.

Pyruvate kinase inhibits proliferation during postnatal cerebellar neurogenesis and suppresses medulloblastoma formation

Katherine Tech[1,2], **Andrey P. Tikunov**[1], **Hamza Farooq**[3,4], **A. Sorana Morrissy**[3,4], **Jessica Meidinger**[2], **Taylor Fish**[2], **Sarah C. Green**[1], **Hedi Liu**[2], **Yisu Li**[5], **Andrew J. Mungall**[5], **Richard A. Moore**[5], **Yussanne Ma**[5], **Steven J.M. Jones**[5], **Marco A. Marra**[5], **Matthew G. Vander Heiden**[6,7], **Michael D. Taylor**[3,4,8,9], **Jeffrey M. Macdonald**[1], and **Timothy R. Gershon**[2,10,11]

[1]Joint Department of Biomedical Engineering, UNC Chapel Hill and NC State University, Chapel Hill, NC 27599, USA

[2]Department of Neurology, University of North Carolina School of Medicine, Chapel Hill, NC 27599, USA

[3]Developmental & Stem Cell Biology Program, The Hospital for Sick Children, Toronto, Ontario M5G 0A4, CAN

[4]The Arthur and Sonia Labatt Brain Tumour Research Centre, The Hospital for Sick Children, Toronto, Ontario M5G 0A4, CAN

[5]Michael Smith Genome Sciences Centre, BC Cancer Agency, Vancouver, BC V5Z 4S6 CAN

[6]David H. Koch Institute for Integrative Cancer Research, Massachusetts Institute of Technology, Cambridge, MA 02139, USA

[7]Dana-Farber Cancer Institute, Boston, MA 02115, USA

[8]Department of Laboratory Medicine and Pathobiology, University of Toronto, Toronto, Ontario M5G 0A4, CAN

[9]Division of Neurosurgery, The Hospital for Sick Children, Toronto, Ontario M5S 3E1, CAN

[10]Lineberger Comprehensive Cancer Center, University of North Carolina School of Medicine, Chapel Hill, NC 27599, USA

[11]UNC Neuroscience Center, University of North Carolina School of Medicine, Chapel Hill, NC 27599, USA

Abstract

Aerobic glycolysis supports proliferation through unresolved mechanisms. We have previously shown that aerobic glycolysis is required for the regulated proliferation of cerebellar granule neuron progenitors (CGNPs), and for the growth of CGNP-derived medulloblastoma. Blocking the initiation of glycolysis via deletion of *Hexokinase-2* (*Hk2*) disrupts CGNP proliferation and restricts medulloblastoma growth. Here, we assessed whether disrupting *Pyruvate kinase-M*

Corresponding Author: Timothy R. Gershon, MD, PhD, Department of Neurology, CB7025, University of North Carolina at Chapel Hill, Chapel Hill, NC 27599, (919) 966-3618, gershont@neurology.unc.edu.

Conflict of Interest: The authors report no financial or non-financial competing interests.

(*Pkm*), an enzyme that acts in the terminal steps of glycolysis, would alter CGNP metabolism, proliferation and tumorigenesis. We observed a dichotomous pattern of PKM expression, in which post-mitotic neurons throughout the brain expressed the constitutively active PKM1 isoform, while neural progenitors and medulloblastomas exclusively expressed the less active PKM2. Isoform-specific *Pkm2* deletion in CGNPs blocked all *Pkm* expression. *Pkm2*-deleted CGNPs showed reduced lactate production and increased SHH-driven proliferation. ^{13}C-flux analysis showed that *Pkm2* deletion reduced the flow of glucose carbons into lactate and glutamate without markedly increasing glucose-to-ribose flux. *Pkm2* deletion accelerated tumor formation in medulloblastoma-prone *ND2:SmoA1* mice, indicating the disrupting PKM releases CGNPs from a tumor-suppressive effect. These findings show that distal and proximal disruptions of glycolysis have opposite effects on proliferation, and that efforts to block the oncogenic effect of aerobic glycolysis must target reactions upstream of PKM.

Introduction

Increased aerobic glycolysis, a common feature of proliferating cells during developmental and malignant growth (1,2), has been proposed as a target for anticancer therapy. CGNPs are transit amplifying cells that proliferate in the postnatal brain (3,4) that utilize aerobic glycolysis during normal brain development (5). CGNPs are also cells-of-origin for SHH-subgroup medulloblastoma (6,7). Medulloblastomas co-opt developmentally-regulated programs of CGNPs (6,7), including the metabolic phenotype of increased aerobic glycolysis (5,8). Understanding how aerobic glycolysis supports CGNP proliferation and medulloblastoma tumorigenesis is essential for designing metabolically-directed medulloblastoma therapies.

During postnatal brain development, CGNPs proliferate in the cerebellum in response to locally secreted Sonic Hedgehog (SHH), generating the largest neuron population in the mammalian brain (9–11). In synchrony with increased CGNP proliferation, SHH signaling induces Hexokinase-2 (HK2) and aerobic glycolysis (5,8). Approximately 30% of medulloblastoma patients show SHH-pathway activation12,13 and mice with activating SHH-pathway mutations develop spontaneous medulloblastomas that recapitulate the human disease (14,15). These tumors arise from CGNPs and, like their cells-of-origin, up-regulate HK2 and aerobic glycolysis (5,8). CGNP proliferation and SHH-driven tumorigenesis in mice typify aerobic glycolysis supporting tumorigenesis arising from developmental growth.

We have previously shown that conditional deletion of *Hk2* in the developing brain blocks SHH-induced aerobic glycolysis, disrupts CGNP differentiation, and reduces medulloblastoma growth, extending the survival of medulloblastoma-prone mice (5). These findings demonstrate the importance of aerobic glycolysis in development and cancer, suggesting that blocking glycolysis through HK2 inhibition may produce a clinically significant anti-tumor effect. Development of selective HK2 inhibitors for anti-cancer therapy however, has been problematic (16). Whether targeting glycolysis downstream of HK2 would similarly inhibit tumor growth is unknown. To determine whether the distal portion of the glycolytic pathway is required for the proliferation of normal and transformed

CGNPs, we analyzed the effect of disrupting pyruvate kinase (PK) during cerebellar neurogenesis and medulloblastoma formation.

While HK2 initiates glycolysis, PK catalyzes the final step, converting phosphoenolpyruvate (PEP) and ADP into pyruvate and ATP (17). *Pkm* is the pyruvate kinase expressed in the brain (18). Alternative splicing of a single exon from *Pkm* gives rise to either *Pkm1*, which includes exon 9, or *Pkm2*, where exon 9 replaces exon 10 (19). PKM1 is constitutively active and typically expressed in differentiated cells, while PKM2 has a regulated activity and is commonly expressed in cancer (20–24). PKM2 can be activated by fructose-1,6-bisphosphate, an upstream glycolytic intermediate (23,24) and inactivated by interaction with tyrosine-phosphorylated proteins responding to growth factor receptor signaling (20,21,25). While the regulated activity of PKM2 may allow proliferating cells to adjust their metabolism to dynamic requirements (2), the specific benefit of low PKM2 activity has not been identified.

PKM2 is expressed in diverse cancers, suggesting a role in cancer growth. Xenograft tumors engineered to overexpress either isoform showed that PKM2 expression confers a relative growth advantage (26). Other studies have reported non-metabolic, growth-promoting functions such as transcriptional regulation (27,28) and histone phosphorylation (29,30). However, isoform-specific deletion studies show that PKM2 is not required for tumor formation. Aged mice with isoform-specific *Pkm2* deletion develop liver cancer (31) and breast cancers are accelerated in *Brca1*-deleted mice with co-deletion of *Pkm2* (32). These studies identify cancers in which *Pkm2* deletion promotes tumor growth. However, neither study showed an effect of *Pkm2* deletion on tumor glycolysis, potentially because PKM2 activity may be fully down-regulated in established tumors. To identify metabolic processes linking *Pkm2* to growth, it is necessary to analyze *Pkm2* deletion in normal proliferative cells that, unlike cancer cells, are not locked into a proliferative state. CGNPs present an ideal opportunity to study *Pkm2* function because these cells can modulate both aerobic glycolysis and proliferation, and are also vulnerable to malignant transformation in medulloblastoma tumorigenesis.

PKM2 is induced by SHH in CGNPs and expressed in the *ND2:SmoA1* mouse model of medulloblastoma (8), suggesting a role in SHH-driven growth. PKM2 up-regulation has also been noted in MYC-amplified Group 3 medulloblastomas (33), suggesting a role for PKM2 in tumor growth across human medulloblastoma subgroups. Here, we analyzed PKM-mediated regulation of CGNP glucose metabolism, proliferation, and tumorigenesis. Like *Hk2* deletion, *Pkm2* deletion decreased CGNP conversion of glucose to lactate. However, unlike *Hk2* deletion, *Pkm2* deletion increased SHH-driven proliferation, and accelerated medulloblastoma formation in mice expressing a constitutively active *Smo* allele. The differential effects of impeding aerobic glycolysis through deletion of *Hk2* or *Pkm2* identify the glycolytic steps upstream of PK as critical to supporting proliferation during development as well as contributing to tumorigenesis.

Materials and Methods

Animals

All wild-type and genetically engineered mice were maintained on the C57/Bl6 background with at least 5 backcrosses. *ND2:SmoA1* mice were provided by Dr. James Olson (Fred Hutchinson Cancer Research Center, Seattle, WA, USA). *Math1-Cre* mice were provided by Dr. David Rowitch (UCSF, CA, USA) and Robert Wechsler-Reya (Sanford-Burnham Medical Research Institute, La Jolla, CA, USA). Eva Anton (UNC-CH, NC, USA) provided *hGFAP-Cre* mice. *Pkm2*$^{fl/fl}$ mice were generously shared by Dr. Matthew Vander Heiden (MIT, Cambridge, MA, USA). Medulloblastoma-prone mice were monitored daily for abnormalities of head shape and movement. At the onset of tumor symptoms, such as weight loss, ataxia, and impaired movement, animals were sacrificed and survival time to onset of symptoms was considered the event-free survival.

For 5-ethynyl-2′-deoxyuridine (EdU) experiments, mice were IP injected with EdU (#A10044, Life Technologies, Grand Island, NY, USA) at 40 mg/kg in 50 μL of HBSS and dissected 24h later. Brains were fixed in 4% paraformaldehyde in 1X PBS for 24h at 4°C, then processed for histology. All animal handling and protocols were carried out in accordance with established NIH practices and approved under UNC IACUC #13-121.0 and 15-306.0.

Cell Culture Techniques

CGNPs were isolated and cultured as previously described (5,34). Briefly, cerebella were dissected from P5 pups, dissociated, and allowed to adhere to coated culture wells in DMEM/F12 (#11320, Life Technologies, Grand Island, NY, USA) with 25 mM KCl, supplemented with FBS and N2. After 4h, media were replaced with identical serum-free media. Cells were maintained in 0.5 μg/mL SHH (#464SH, R&D Systems, Minneapolis, MN, USA) or vehicle (0.1% BSA in 1X PBS). Where indicated, vismodegib (#S1082, Selleck Chemicals, Houston, TX, USA) was added to cultures after the first 24h, at the specified concentration, with cells harvested 24h after drug treatment. *In vitro* CGNP proliferation was measured by EdU incorporation after a 1h exposure to 20 μM EdU. EdU was visualized following the manufacturer's protocol (#C10337, Life Technologies). Cell counts were performed using Leica-Metamorph software (Molecular Devices, Sunnyvale, CA, USA). No cell lines were use in these studies.

In vitro metabolism studies

^{1}H NMR and LC-MS acquisition methods are described in detail in the Supplementary Materials and Methods. Briefly, CGNPs of each genotype were cultured in at least 3 replicate wells. Explanted CGNPs were maintained in [1,6-^{13}C] glucose media for 24h followed by media sampling and cell extraction for metabolomic analysis. We normalized to cell number at 24 hours to account for differences in growth rates by counting cells in a replicate set of wells cultured in parallel.

For the enzymatic measurement of lactate, media from at least three replicate wells were sampled at the specified time points and lactate was quantified using the L-Lactate Assay Kit (#1200011002, Eton Bioscience, San Diego, CA, USA) per manufacturer's protocol.

For PK activity assays, cells from at least three replicate wells per condition, or whole cerebella from at least three replicate mice per genotype, were lysed and processed for the colorimetric assay per manufacturer's protocol (#K709-100, BioVision Inc., Milpitas, CA, USA).

Histology and immunohistochemistry

Mouse brain and tumor tissues were processed for immunohistochemistry (IHC) as previously described[35] using antibodies listed in Supplementary Materials and Methods. EdU was visualized per manufacturer's protocol. After IHC and EdU staining, where indicated, nuclei were counterstained with 200 ng/mL 4′6-diamidino-2-phenylindole (DAPI; #D1306, ThermoFisher Scientific, Waltham, MA, USA) in 1X PBS for 5 min. Stained slides were digitally acquired using an Aperio ScanScope XT (Aperio, Vista, CA, USA). Where indicated, maximum intensity projections of stained tissue sections were acquired on a Zeiss LSM 780 confocal microscope with a Plan-Apochromat 20× objective (NA 0.8). To quantify EdU, Proliferating Cell Nuclear Antigen (PCNA), and $p27^{Kip1}$ positive cells in the EGL, the EGL region was manually annotated on each section, which was then subjected to automated cell counting using Tissue Studio (Definiens, München, Germany) for fluorescent slides. For premalignant lesion analysis, the entire cerebellum was annotated and used for cell counts.

Western blot analysis

Cultured cells and whole cerebella were lysed by homogenization in RIPA buffer containing protease inhibitor cocktail, NaF, and sodium orthovanadate. Protein concentrations were quantified using the bicinchoninic acid (BCA) method (#23229, ThermoFisher Scientific) and equal concentrations of protein were resolved on SDS-polyacrylamide gels followed by transfer onto polyvinylidene difluoride membranes. Immunologic analysis was performed on the SNAP i.d. Protein Detection System (Millipore, Billerica, MA, USA) per manufacturer's protocol with antibodies listed in Supplementary.

Materials and Methods—Western blots were developed using the enhanced chemiluminescent SuperSignal West Femto Maximum Sensitivity Substrate (#34095, ThermoFisher Scientific) and digitized using the C-DiGit blot scanner (LI-COR, Lincoln, NE, USA). Quantification was performed using Image Studio Lite software (LI-COR).

DNA sequencing

DNA was lysed from toe cuttings and used to generate *Pkm2* PCR products. *Pkm2* PCR primers were F_TAGGGCAGGACCAAAGGATTCCCT and R_CTGGCCCAGAGCCACTCACTCTTG. PCR products were extracted from a 0.8% agarose gel using the MinElute Gel Extraction Kit (#28604, Qiagen, Valencia, CA, USA), cloned by TOPO TA Cloning (#K4575-J10, Life Technologies) and sequenced from the M13F and M13R primer sites by Sanger sequencing (Eton Bioscience).

Patients and samples

All patient samples were obtained with consent as outlined by individual institutional review boards. Written informed consent was obtained at the time of surgical resection. De-identified medulloblastoma tissues were obtained from Queensland Children's Tumor Bank (Brisbane, Australia), German Cancer Research Center (Heidelberg, Germany), Sanford-Burnham Medical Research Institute (La Jolla, USA), and Hospital for Sick Children (Toronto, Canada).

Differential Pkm isoform expression analysis of RNA-seq data

Library construction, sequencing, and alignment of RNA-seq data are described in detail in the Supplementary Materials and Methods. Transcriptome aligned binary alignment files (bams) were processed using RNA-Seq by Expectation Maximization (RSEM) software (36). The reference for RSEM was built using the same GRCh37-lite assembly and GRCh37.75 GTF as used by STAR aligner (37). This was followed by the calculation of PKM isoform level FPKM using RSEM with default parameters in 97 human tumors. The accession number for the RNA-seq data is European Genome-phenome Archive: EGAD00001001899.

Survival analysis of SHH-subgroup medulloblastoma patients

PKM2 FPKM expression was converted to a Z-score and used to segregate SHH patients into a high or low category with the criteria of being greater than 0.5 or smaller than −0.5 respectively. A cox proportional hazard model was used to determine the presence of a survival difference.

Results

Pkm isoform expression in the brain mirrors differentiation status

We found dichotomous *Pkm* isoform expression in the postnatal brain that varied with differentiation state. was in Differentiated neurons throughout the brain expressed PKM1 and not PKM2 (Fig. 1A). In contrast, neural progenitors of the cerebellar external granule layer (EGL), hippocampus (HC), and subventricular zone/rostral migratory stream (SVZ/RMS) expressed PKM2 and not PKM1 (Fig. 1B).

The temporal expression of PKM2 in the cerebellum coincided with postnatal neurogenesis. CGNP proliferation peaks at postnatal day 7 (P7) and ends by P15, as CGNPs progressively exit the cell cycle, migrate to the internal granule layer (IGL), and differentiate into cerebellar granule neurons (CGNs) (3,4,7). Western blot of whole cerebellum lysates showed that PKM2, like the CGNP proliferation marker Cyclin-D2 (CCND2), decreased between P7 and P15, while PKM1 conversely increased (Fig. 1C). PKM2 was not limited to proliferating progenitors; both proliferating, PCNA+ CGNPs in the outer layer of the EGL (oEGL), and differentiating, PCNA− CGNPs of the inner EGL (iEGL) expressed PKM2 (Fig. 1D). Similarly, in the SVZ/RMS, both PCNA+ and PCNA- progenitors expressed PKM2 (Fig. 1E). Thus, PKM2 marked undifferentiated brain progenitors, whether proliferating or quiescent, while PKM1 marked differentiated neurons.

To determine if medulloblastomas, like CGNPs, exclusively expressed PKM2, we analyzed PKM isoform expression in transgenic, medulloblastoma-prone *ND2:SmoA1* mice. *ND2:SmoA1* mice express a mutant, constitutively active allele of *Smo*, driven by the *NeuroD2* promoter. In CGNPs of *ND2:SmoA1* mice, SHH-pathway activation prolongs proliferation beyond P15. These mice develop medulloblastoma with incomplete penetrance after a variable latency (14). During this latent period, CGNPs continue to proliferate in premalignant lesions within the EGL, generating progeny that differentiate, undergo apoptosis, or remain proliferative.

We found that CGNPs in premalignant lesions of P60 *ND2:SmoA1* mice expressed PKM2 and not PKM1 (Fig. 1F). Similarly, medulloblastomas derived from these premalignant lesions consistently and homogeneously expressed PKM2, while adjacent, normal brain expressed PKM1 (Fig. 1G). We compared the expression of PKM1 and PKM2 mRNA in human medulloblastoma samples by RNA-seq. As in the mouse model, we found exclusive expression of PKM2, with minimal PKM1 in all four medulloblastoma subgroups (Fig. 1H). Together, our studies of mouse and human tumors show that developmental PKM2 expression persists throughout medulloblastoma tumorigenesis.

SHH stimulates PKM2 expression

To examine the effect of SHH signaling on PKM1/2 expression, we isolated CGNPs and compared PKM isoform expression in the presence or absence of SHH ligand. We labeled S-phase cells by adding EdU to CGNP cultures 1h before fixation. EdU+ and PKM2+ cells were more numerous in SHH-treated wells (Fig. 2A; cyan arrows) compared to SHH-deprived controls (Fig. 2B; arrows). In SHH-treated wells, PKM2 was detected in both EdU + and EdU− cells (Figs. 2A,B; white arrowheads). Consistent with the absence of PKM1 in the EGL, no CGNPs in either condition showed detectable PKM1; rare cells that were PKM1+ did not have morphology characteristic of CGNPs (Figs. 2C,D). These data show that SHH sustained PKM2 expression in CGNPs, while PKM1 expression remained low during the initiation of differentiation in SHH-deprived CGNPs.

To determine the effect of SHH inhibition on PKM expression, we analyzed SHH-treated CGNPs exposed to the *Smo* inhibitor vismodegib (38) by quantitative PKM Western blot. As an indicator of SHH-driven proliferation, we also measured CCND2 expression. SHH-treated CGNP explants demonstrated 5.5-fold more CCND2 compared to SHH-deprived CGNPs, and 2-fold more PKM2 (Fig. 2E). PKM1, which likely originated from rare cells detected by IHC (Figs. 2C,D) was also significantly increased SHH-treated explants. Vismodegib decreased CCND2 by 30% but did not significantly alter PKM1 or PKM2 expression (Fig. 2E). Thus, both PKM2 and CCND2 were up-regulated by SHH, but compared to *CcnD2*, *Pkm* was markedly less responsive to changes in SHH signaling. These data suggest that *Pkm*, unlike *CcnD2* (11), is not a direct SHH target.

PK activity in CGNPs is increased by growth stimulation

Tyrosine kinase signaling, and specifically insulin signaling, can down-regulate PKM2 catalytic activity in diverse cell lines (21,39,40). While CGNPs are typically cultured with insulin-rich N2 supplement to improve cell viability (41), we have shown that CGNPs can

be cultured without N2 for 24h, reducing IGFR activation without compromising survival (5). We maintained CGNPs in the presence or absence of SHH or N2, to determine the effect of SHH/IGFR co-stimulation on Pkm expression and PK activity in CGNPs.

We found that SHH/IGFR co-stimulation was required for CGNP aerobic glycolysis, as N2 deprivation reduced lactate production (Fig. 2F) in a manner comparable to SHH-withdrawal[5]. We have shown that growth factor stimulation induces aerobic glycolysis through a complex program that depends on many genes, including N-myc and Hk2 (5). To determine if this program may include changes in PK activity and PKM expression, we analyzed CGNPs cultured with or without SHH or N2. N2-deprivation potently inhibited IGF signaling, resulting in a 70% reduction in AKT phosphorylation, and more modestly reduced PKM2 expression by 30% (Supplementary Fig. S1). By measuring the conversion of exogenous PEP to pyruvate in CGNP lysates, we found that CGNPs maintained with SHH+N2 showed significantly higher PK activity compared to either SHH without N2 or N2 without SHH (Figs. 2G,H). These findings show that CGNP PK activity and PKM2 expression were responsive to extracellular signaling, and were maximal with SHH/IGFR co-activation, thus varying directly with glycolysis. While reduced PK activity has been correlated with growth factor stimulation in cancer cells (20,25,26), in CGNPs, developmentally-relevant growth factors increased PKM2 expression, PK activity, and aerobic glycolysis.

Pkm2 deletion is not replaced by Pkm1 in brain progenitors

To determine the developmental significance of PKM in CGNPs, we examined the effect of conditionally deleting the *Pkm2*-specific exon 10 (19). We crossed *Math1-Cre* mice, which express Cre recombinase in CGNPs (42,43), with $Pkm2^{fl}$ mice that harbor loxP sites flanking *Pkm* exon 10[32]. The resulting *Math1-Cre;*$Pkm2^{fl/fl}$ mice ($Pkm2^{cKO}$) mice were viable and fertile without neurologic deficits. $Pkm2^{cKO}$ cerebellum showed normal foliation and cellular organization, without PKM2 or PKM1 in the EGL (Fig. 3A,B). PKM1 expression was increased in IGL of $Pkm2^{cKO}$ mice, which is populated by CGNs that derive from CGNPs and inherit the deletion of exon 10 (Fig. 3A). Thus, *Pkm2* deletion in the Math1 lineage did not induce compensatory PKM1 in progenitors but did increase PKM1 expression by terminally differentiated neurons. Consistent with these changes, Western blot showed reduced PKM2 and increased PKM1 in P7 $Pkm2^{cKO}$ cerebella compared to no-Cre littermate controls (Fig. 3C). In whole cerebellum lysates, PK activity was equivalent in $Pkm2^{cKO}$ and littermate controls (Fig. 3D). In CGNPs, however, *Pkm2* deletion blocked all detectable PKM expression.

During the breeding of $Pkm2^{cKO}$ mice, we noted an unanticipated tendency for germline recombination of the $Pkm2^{fl}$ allele. This recombination event was detected as a smaller-than-expected PCR product when primers flanking *Pkm* exon 10 were used to amplify genomic DNA. While these primers were separated by 605 bp in the $Pkm2^{fl/fl}$ allele and 560 bp in the $Pkm2^{+/+}$ allele, we found pups in several litters that generated 220 bp PCR products consistent with the recombined allele (Supplementary Fig. S2A). Sequencing of this band demonstrated that intron 9–10 and 10–11 were brought together, separated by a single loxP site, consistent with Cre-mediated excision of exon 10 from *Pkm* (32)

(Supplementary Fig. S2B). Similar germline recombination has been observed when *Pkm2*^{fl} mice were crossed with other non-germline Cre drivers (M. Vander Heiden, unpublished), suggesting that *Pkm* exon 10 deletion is positively selected in the germline. The recombined allele (*Pkm2*^{null}) was heritable and *Pkm2*$^{null/null}$ mice were viable and fertile without neurologic abnormalities, consistent with the published *Pkm2* null phenotype (31). *Pkm2* null mice have been reported to develop spontaneous hepatocellular carcinoma in the second year of life (31), however, we did not observe any spontaneous tumor formation in our *Pkm2*$^{null/null}$ aged up to one year. In *Pkm2*$^{null/null}$ mice, PKM2 was absent from all brain cells, while PKM1 was appropriately limited to differentiated neurons (Supplementary Fig. S2C,D). Like *Pkm2*^{cKO} mice, *Pkm2*$^{null/null}$ mice showed normal brain anatomy.

Pkm2 deletion increases CGNP proliferation

Although *Pkm2*^{cKO} cerebella had normal organization, quantitative analysis showed that CGNP proliferation was increased compared to PKM2-intact littermate controls. We analyzed proliferation dynamics *in vivo*, by injecting EdU at P6 into *Pkm2*^{cKO} and *Pkm2*$^{fl/fl}$ no-Cre littermates. We harvested cerebella 24h after EdU injection and quantified the number of EdU+ cells in the EGL that expressed the CGNP differentiation marker p27^{Kip1}. Both genotypes included differentiating, EdU+p27 ^{Kip1}+ CGNPs and proliferating, EdU +p27^{Kip1}−CGNPs (Figs. 4A,B). While EdU labeling was similar between genotypes (Fig. 4C), we noted a trend toward reduced p27^{Kip1} labeling in *Pkm2*^{cKO} CGNPs (Fig. 4D). Importantly, EdU+ CGNPs that were p27^{Kip1}- were more numerous in the EGL of *Pkm2*^{cKO} mice (Fig. 4E). *In vitro* studies provided additional evidence of increased proliferation with *Pkm2* deletion, as CGNPs explanted from *Pkm2*^{cKO} mice showed a higher fraction of EdU+ cells after a 1h pulse, compared to CGNPs explanted from littermate controls (Fig. 4F).

Consistent with increased proliferation of *Pkm2*^{cKO} CGNPs, analysis of equivalent midline cerebellar sections showed that *Pkm2*^{cKO} cerebella contained significantly more cells (CGNPs and CGNs) compared to littermate controls (Fig. 4G). The ratio of EGL:IGL was not significantly different between genotypes however (Fig. 4H), indicating that *Pkm2* deletion did not prevent CGNPs from progressing through their normal differentiation trajectory. Thus, *Pkm2* deletion blocks all PKM expression in CGNPs, with the effects of increasing proliferation and reducing cell cycle exit, without altering cell fate.

Pkm2 deletion inhibits the catabolism of glucose to lactate

We used a non-biased, metabolomic approach to determine the effect of *Pkm2* deletion and consequent loss of PKM function on CGNP metabolism. We isolated CGNPs from P5 *Pkm2*^{cKO} mice and littermate controls and cultured them in three replicate wells for 24h in media with [1,6-^{13}C] glucose replacing unlabeled glucose. We analyzed media metabolites from each replicate well for each condition at 0 and 24h using NMR spectroscopy followed by orthogonal partial least squares discriminant analysis to identify species with metabolic rates that varied consistently across genotypes (Supplementary Table S1).

Lactate production was significantly reduced in *Pkm2*^{cKO} CGNPs compared to controls (Fig. 5A). Lactate was the species with the largest change in metabolic rate in *Pkm2*^{cKO} CGNPs versus controls (Supplementary Table S1). Lactate production and arginine

utilization were both significantly reduced in the *Pkm2*-deleted cells, but the change in arginine was 10-fold smaller and unlikely to be directly related to glucose metabolism. We confirmed that *Pkm2*^{cKO} CGNPs produced less lactate by measuring media lactate in replicate wells by colorimetric assay (Fig. 5B). The ^{13}C fractional enrichment of lactate was also decreased in *Pkm2*^{cKO} CGNPs (Figs. 5C,D), showing that a smaller proportion of utilized glucose was converted to lactate.

To determine how *Pkm2* deletion altered the intracellular disposition of glucose in CGNPs, we analyzed cell extracts by liquid chromatography-mass spectrometry (LC-MS). Diverse molecules detected by LC-MS detected did not show significantly different distribution between genotypes. We noted a trend toward increased choline in Pkm2^{cKO} CGNPs; this trend cannot be directly related to glucose metabolism, but is consistent with increased proliferation (Fig. 5E). We were able to detect ^{13}C-labeling in glutamate, which we used as a measure of flow through the Krebs cycle, and in the ribose component of ATP, ADP and AMP, which we used as a measure of flow through the pentose phosphate pathway (PPP) (Fig. 6).

Relative to *Pkm2*-intact controls, *Pkm2*^{cKO} CGNPs showed a small, but statistically significant decrease in glutamate with 3 or 4 ^{13}C atoms (Fig. 6). The incorporation of multiple ^{13}C atoms from [1,6-^{13}C] glucose requires both conversion of pyruvate to acetyl-CoA by PDH and multiple turns of the Krebs cycle (Supplementary Fig. S3). The reduced glutamate with 3 or 4 ^{13}C atoms in controls indicates that that PKM2 deletion marginally reduced labeling downstream of PDH, consistent with a shift in fate of glucose-derived carbons.

Both genotypes demonstrated ^{13}C incorporation into ribose. LC-MS demonstrated labeled parent masses of ATP, ADP, and AMP that fragmented into unlabeled adenine and ^{13}C-labeled ribose. These data demonstrate active flow through the PPP. However, we did not detect a robust difference in PPP flux between genotypes (Fig. 6). These data suggest that unidentified reactions in *Pkm2*^{cKO} CGNPs bypass the conversion of PEP to pyruvate, allowing the incorporation of ^{13}C into glutamate and lactate at a reduced but detectable rate, while maintaining comparable flow through the PPP. In net, *Pkm2* deletion redirected glucose-derived metabolites away from both lactate generation and retention in the Krebs cycle, without causing a large increase in PPP flux.

Medulloblastoma tumorigenesis is exacerbated by loss of PKM2

We examined the functional consequence of *Pkm2* deletion on SHH-driven medulloblastoma tumorigenesis by crossing *Pkm2*^{cKO} and *Pkm2*$^{null/null}$ mice with medulloblastoma-prone mouse lines. We generated tumor-prone mice using either the *SmoM2* allele that induces rapidly developing progressive medulloblastoma with 100% incidence by P20, or with the *ND2:SmoA1* allele that induces tumors more slowly. In contrast to the anti-tumor effect of *Hk2* deletion, we found that *Pkm2* deletion did not slow tumor progression in *Math1-Cre;SmoM2;Pkm2*$^{fl/null}$ mice (Fig. 7A) or *hGFAP-cre;SmoM2;Pkm2*$^{fl/null}$ mice (data not shown) compared to *Pkm2*-intact, littermate controls. In both of these models, however, rapid tumor growth limits the ability to determine whether PKM2 ablation accelerates disease. To address this question, we examined *Pkm2* deletion in *ND2:SmoA1* mice.

ND2:SmoA1 mice with *Pkm2* deletion developed tumors more frequently than *Pkm2*-intact *ND2:SmoA1* controls. We compared *ND2:SmoA1* mice with two mutant copies of *Pkm2*, including *Math1-Cre;ND2:SmoA1;Pkm2*$^{fl/fl}$, *Math1-Cre;ND2:SmoA1;Pkm2*$^{fl/null}$, and *ND2:SmoA1;Pkm2*$^{null/null}$ genotypes to control *ND2:SmoA1* mice with two intact copies of *Pkm2*, including no-*Cre;ND2:SmoA1;Pkm2*$^{+/+}$, no-*Cre;ND2:SmoA1;Pkm2*$^{fl/+}$, and *Math1-Cre;ND2:SmoA1;Pkm2*$^{+/+}$ genotypes. We observed a trend toward increased tumor formation in *Pkm2*–deleted mice at P150, where the incidence was 37.5% with *Pkm2* deletion vs 15.8% for controls (p=0.245, Fisher's Exact test). By 300, tumor incidence was 100% in *Pkm2*-deleted mice versus 57.9% for controls (p=0.004, Fisher's Exact test). Consistently, *ND2:SmoA1* mice with *Pkm2* deletion demonstrated significantly shorter progression-free survival (Fig. 7B).

To determine if *Pkm2* deletion accelerated tumor growth through a cell autonomous process, we separately compared the *Math1-Cre;ND2:SmoA1;Pkm2*$^{fl/null}$ and *ND2:SmoA1;Pkm2*$^{null/null}$ subgroups to *Pkm2*-intact *ND2:SmoA1* controls. This analysis also showed significantly shorter survival for both *Math1-Cre;ND2:SmoA1;Pkm2*$^{fl/null}$ (Fig. 7C) and *ND2:SmoA1;Pkm2*$^{null/null}$ genotypes (Fig. 7D). We found no statistically significant difference between different *Pkm2*-deleted genotypes. Thus, the accelerating effect of *Pkm2* deletion on *SmoA1*-driven tumorigenesis was cell autonomous.

Like *Pkm2*-deleted CGNPs, *Pkm2*-deleted medulloblastoma cells expressed neither PKM2 (Fig. 7E) or PKM1 (Fig. 7F). However, we noted scattered PKM1+ cells within *Pkm2*-deleted tumors (Fig. 7E'"). These cells were consistently PCNA- (Supplementary Fig. S4) and were also found in *Pkm2*-intact tumors. These non-proliferative, PKM1+ cells may be entrapped neurons or differentiated progeny of tumor cells. Similar PKM1+ stromal cells were previously observed in *Pkm2*-deleted breast tumors (32).

The slow process of tumor formation in *ND2:SmoA1* mice allowed us to analyze the effect of *Pkm2* deletion on the growth of premalignant lesions. We counted PCNA+ cells in cerebella of *ND2:SmoA1* mice with deleted or intact *Pkm2*, harvested at either P60 or P120 and normalized the number of PCNA+ cells to the total number of cells in each cerebellar section (Fig. 7G). In controls, the median fraction of PCNA+ cells in the cerebellum and the range of these values decreased over time, consistent with a dynamic balance between growth and growth suppression. In contrast, in *Pkm2*-deleted genotypes, the median and range of PCNA+ fractions increased over time, consistent with reduced growth suppression during the premalignant period. Altogether, *Pkm2* deletion increased SHH-driven CGNP proliferation during development, accelerated tumorigenesis in premalignant lesions in *Smo*-mutant mice, and increased the incidence of tumor formation from these lesions.

The more rapid progression of mouse tumors with *Pkm2* deletion was mirrored by a trend toward shorter survival in medulloblastoma patients with low PKM2 expression. We classified SHH-subgroup medulloblastoma patients as having either high or low PKM2 expressing tumors and compared their clinical outcomes. All patients were treated similarly with radiation and chemotherapy. While not statistically significant, we found that patients with low PKM2 expression trended toward shorter survival times (Fig. 7H). Together, these

data confirm that PKM2 is not essential for tumor progression and suggest that low PKM2 expression, like *Pkm2* deletion, enhances medulloblastoma tumor growth.

Discussion

We analyzed the functional significance of pyruvate kinase isoform expression in the developing brain and in medulloblastoma. While aerobic glycolysis has been associated with proliferation in both development (5,44) and cancer (1,2), our data show that disrupting glycolysis at PK increases, rather than decreases both developmental proliferation and tumorigenesis. We show that within the neural lineage, *Pkm* is spliced into mutually exclusive expression patterns that correlate PK activity with differentiation state. In the postnatal brain, undifferentiated progenitors in the cerebellum, hippocampus, and SVZ expressed the less active PKM2 isoform, while differentiated neurons expressed the more active PKM1. The correlation of PKM2 with the undifferentiated state was maintained in medulloblastoma. The PKM1:PKM2 dichotomy persisted after conditional or germline deletion of *Pkm2*, which increased PKM1 in differentiated cells but not in progenitors. The lack of compensatory up-regulation of PKM1 in brain progenitors contrasts with prior observations in MEFs and other tissues, where PKM1 expression increases on *Pkm* exon 10 deletion (31,45). In *Pkm2*-deleted MEFs, increased PKM1 caused nucleotide scarcity and cell cycle arrest. However, $Pkm2^{cKO}$ CGNPs expressed neither PKM isoform, showed decreased conversion of glucose to lactate and increased proliferation. *Pkm2* deletion also enhanced the growth of premalignant lesions and tumors in *ND2:SmoA1* mice. These findings demonstrate that the absence of detectable PKM2 in $Pkm2^{cKO}$ mice increased developmental proliferation and neural progenitor susceptibility to tumorigenesis.

The different effects of *Pkm2* deletion in CGNPs and MEFs argue that proliferation is restricted by PKM1, rather than enhanced by PKM2. We propose that high PK activity inhibits SHH-driven proliferation and suppresses tumor formation. Consistent with this model, splicing *Pkm* to PKM2 has a permissive effect on proliferation and abrogating PKM expression is more permissive. The finding that SHH/IGFR co-signaling increased CGNP PK activity is not necessarily inconsistent with this model as growth factors are known to induce simultaneously both positive and negative regulation of proliferation in primary cells. For example, SHH activation induces Patched (Ptc) expression in CGNPs, which negatively regulates SHH signaling (46,47). Activating PKM2 may be a similar inhibitory element within the normal regulation of SHH-induced growth in primary cells.

Our prior *Hk2* deletion studies demonstrate that the initiation of glycolysis supports postnatal neurogenesis and sustains the malignant growth of medulloblastomas. In contrast, our present studies of *Pkm2* deletion show that impeding the flow of glucose to lactate increases CGNP proliferation and accelerates medulloblastoma tumorigenesis. Together, these deletion studies show that the pathways through which glucose is metabolized significantly influence the proliferative behavior of undifferentiated cells. The divergent effects of *Hk2* deletion versus *Pkm2* deletion establish the glycolytic steps upstream of PK as critical to supporting the proliferative phenotype of neural progenitors and cognate tumors.

Between the reactions catalyzed by HK2 and PKM2 are several reversible reactions that permit glycolytic intermediates to be shunted toward biosynthetic processes. We and others have previously proposed that low flow downstream of PEP, achieved by preferentially splicing PKM to generate PKM2, may support growth by diverting glycolytic intermediates away from lactate generation and towards the synthesis of macromolecules (2,48,49). However, evidence for decreased lactate and increased anabolism with *Pkm2* deletion was lacking in *Pkm2*-deleted breast tumors (32) and MEFs (45). Recent work found that the direct incorporation of glucose carbons is a minor component of the biomass of proliferating cancer cells (50). Working with primary neural progenitors limited the amount of material for analysis and thus the range of metabolites we could detect. However, we were able to detect ^{13}C in extracellular lactate and in intracellular glutamate and ribose. *Pkm2* deletion decreased the incorporation of glucose into lactate and glutamate, suggesting that that altering PEP metabolism redirects glucose carbons to different metabolic fates. *Pkm2* deletion did not produce a detectable effect on the incorporation of glucose into ribose, suggesting that PPP flux is not the major destination of glucose carbons redirected by low PK activity.

Our ^{13}C studies show that CGNPs lacking both PKM1 and PKM2 can metabolize glucose to pyruvate, raising the question of what alternative pathway metabolizes PEP. We were not able to detect changes in glycolytic intermediates that might indicate how PEP is processed in $Pkm2^{cKO}$ CGNPs. However, prior studies have shown that PKM2-expressing cells with low PK activity can generate pyruvate by transferring the high-energy phosphate of PEP to the enzyme PGAM1(51). This phosphorylation activates PGAM1, which may promote biosynthetic metabolism (52). If PEP-PGAM1 phosphotransfer occurs in CGNPs, it may mediate the growth promoting effect of PKM2 splicing that is enhanced by *Pkm2* deletion.

Our work suggests that *Pkm* functions as a tumor suppressor. Identifying *Pkm* as a tumor suppressor has profound implications for aerobic glycolysis and may be effectively targeted in cancer treatment. Inhibiting PKM function as an anti-cancer therapy would be counterproductive while drugs that increase PKM catalytic activity may be of limited therapeutic value if tumors can thrive with low PKM expression. The loss of tumor suppressor genes, however, may be targeted through alternative approaches that require defining the consequent changes in pathway regulation (53,54). A detailed understanding of how low PK activity promotes proliferation may produce novel clinical strategies to treat tumor growth.

Supplementary Material

Refer to Web version on PubMed Central for supplementary material.

Acknowledgments

We thank the UNC CGBID Histology Core supported by P30 DK 034987, the UNC Tissue Pathology Laboratory Core supported by NCI CA016086 and UNC UCRF, and the UNC Neuroscience Center Confocal and Multiphoton Imaging facilities for providing expertise in immunohistochemistry and confocal imaging. This work was supported by the National Institute of Neurologic Disorder and Stroke (R01NS088219) and by the American Institute for Cancer Research.

Financial support: K Tech, JM Macdonald and TR Gershon were supported by the National Institute of Neurologic Disorder and Stroke (R01NS088219). K Tech and TR Gershon were supported by the American Institute for Cancer Research.

References

1. Warburg O. On the Origin of Cancer Cells. Science. 1956; 123:309–14. [PubMed: 13298683]
2. Lunt SY, Vander Heiden MG. Aerobic Glycolysis: Meeting the Metabolic Requirements of Cell Proliferation. Annu Rev Cell Dev Biol. 2011; 27:441–64. [PubMed: 21985671]
3. Hatten ME, Rifkin DB, Furie MB, Mason CA, Liem RK. Biochemistry of granule cell migration in developing mouse cerebellum. Prog Clin Biol Res. 1982; 85:509–19. [PubMed: 6750635]
4. Hatten ME, Alder J, Zimmerman K, Heintz N. Genes involved in cerebellar cell specification and differentiation. Curr Opin Neurobiol. 1997; 7:40–7. [PubMed: 9039803]
5. Gershon TR, Crowther AJ, Tikunov A, Garcia I, Annis R, Yuan H, et al. Hexokinase-2-mediated aerobic glycolysis is integral to cerebellar neurogenesis and pathogenesis of medulloblastoma. Cancer Metab. 2013; 1:1–17. [PubMed: 24280107]
6. Marino S. Medulloblastoma: developmental mechanisms out of control. Trends Mol Med. 2005; 11:17–22. [PubMed: 15649818]
7. Roussel MF, Hatten ME. Cerebellum: Development and Medulloblastoma. Curr Top Dev Biol. 2011; 94:235–82. [PubMed: 21295689]
8. Bhatia B, Potts CR, Guldal C, Choi S, Korshunov A, Pfister S, et al. Hedgehog-mediated regulation of PPARγ controls metabolic patterns in neural precursors and shh-driven medulloblastoma. Acta Neuropathol. 2012; 123:587–600. [PubMed: 22407012]
9. Dahmane N, Ruiz i Altaba A. Sonic hedgehog regulates the growth and patterning of the cerebellum. Development. 1999; 126:3089–100. [PubMed: 10375501]
10. Wechsler-Reya RJ, Scott MP. Control of Neuronal Precursor Proliferation in the Cerebellum by Sonic Hedgehog. Neuron. 1999; 22:103–14. [PubMed: 10027293]
11. Kenney AM, Rowitch DH. Sonic hedgehog Promotes G1 Cyclin Expression and Sustained Cell Cycle Progression in Mammalian Neuronal Precursors. Mol Cell Biol. 2000; 20:9055–67. [PubMed: 11074003]
12. Kool M, Korshunov A, Remke M, Jones DTW, Schlanstein M, Northcott PA, et al. Molecular subgroups of medulloblastoma: an international meta-analysis of transcriptome, genetic aberrations, and clinical data of WNT, SHH, Group 3, and Group 4 medulloblastomas. Acta Neuropathol. 2012; 123:473–84. [PubMed: 22358457]
13. Northcott PA, Korshunov A, Witt H, Hielscher T, Eberhart CG, Mack S, et al. Medulloblastoma comprises four distinct molecular variants. J Clin Oncol. 2011; 29:1408–14. [PubMed: 20823417]
14. Hallahan AR, Pritchard JI, Hansen S, Benson M, Stoeck J, Hatton BA, et al. The SmoA1 Mouse Model Reveals That Notch Signaling Is Critical for the Growth and Survival of Sonic Hedgehog-Induced Medulloblastomas. Cancer Res. 2004; 21:7794–800.
15. Mao J, Ligon KL, Rakhlin EY, Thayer SP, Bronson RT, Rowitch D, et al. A Novel Somatic Mouse Model to Survey Tumorigenic Potential Applied to the Hedgehog Pathway. Cancer Res. 2006; 66:10171–8. [PubMed: 17047082]
16. Lin H, Zeng J, Xie R, Schulz MJ, Tedesco R, Qu J, et al. Discovery of a Novel 2,6-Disubstituted Glucosamine Series of Potent and Selective Hexokinase 2 Inhibitors. ACS Med Chem Lett. 2016; 7:217–22. [PubMed: 26985301]
17. Lehninger, AL. Lehninger Principles of Biochemistry. 4th. Nelson, DL., Cox, MM., editors. New York, USA: W.H. Freeman; 2005.
18. Imamura K, Tanaka T. Multimolecular Forms of Pyruvate Kinase from Rat and Other Mammalian Tissues. J Biochem. 1972; 71:1043–51. [PubMed: 4342282]
19. Noguchi T, Inoue H, Tanaka T. The M1- and M2-type Isozymes of Rat Pyruvate Kinase Are Produced from the Same Gene by Alternative RNA Splicing. J Biol Chem. 1986; 261:13807–12. [PubMed: 3020052]

20. Varghese B, Swaminathan G, Plotnikov A, Tzimas C, Yang N, Rui H, et al. Prolactin Inhibits Activity of Pyruvate Kinase M2 to Stimulate Cell Proliferation. Mol Endocrinol. 2010; 24:2356–65. [PubMed: 20962042]
21. Christofk HR, Vander Heiden MG, Wu N, Asara JM, Cantley LC. Pyruvate kinase M2 is a phosphotyrosine-binding protein. Nature. 2008; 452:181–8. [PubMed: 18337815]
22. Anastasiou D, Yu Y, Israelsen WJ, Jiang J-K, Boxer MB, Hong BS, et al. Pyruvate kinase M2 activators promote tetramer formation and suppress tumorigenesis. Nat Chem Biol. 2012; 8:839–47. [PubMed: 22922757]
23. Ikeda Y, Noguchi T. Allosteric regulation of pyruvate kinase M2 isozyme involves a cysteine residue in the intersubunit contact. J Biol Chem. 1998; 273:12227–33. [PubMed: 9575171]
24. Ashizawa K, Willingham MC, Liang CM, Cheng SY. In vivo regulation of monomer-tetramer conversion of pyruvate kinase subtype M2 by glucose is mediated via fructose 1,6-bisphosphate. J Biol Chem. 1991; 266:16842–6. [PubMed: 1885610]
25. Hitosugi T, Kang S, Vander Heiden MG, Chung T-W, Elf S, Lythgoe K, et al. Tyrosine phosphorylation inhibits PKM2 to promote the Warburg effect and tumor growth. Sci Signal. 2009; 2:1–8.
26. Christofk HR, Vander Heiden MG, Harris MH, Ramanathan A, Gerszten RE, Wei R, et al. The M2 splice isoform of pyruvate kinase is important for cancer metabolism and tumour growth. Nature. 2008; 452:230–4. [PubMed: 18337823]
27. Gao X, Wang H, Yang JJ, Liu X, Liu Z-R. Pyruvate kinase M2 regulates gene transcription by acting as a protein kinase. Mol Cell. 2012; 45:598–609. [PubMed: 22306293]
28. Yang W, Xia Y, Ji H, Zheng Y, Liang J, Huang W, et al. Nuclear PkM2 regulates beta-catenin transactivation upon EGFR activation. Nature. 2011; 480:118–22. [PubMed: 22056988]
29. Yang W, Xia Y, Hawke D, Li X, Liang J, Xing D, et al. PKM2 Phosphorylates Histone H3 and Promotes Gene Transcription and Tumorigenesis. Cell. 2012; 150:685–96. [PubMed: 22901803]
30. Ignacak J, Stachurska MB. The dual activity of pyruvate kinase type M2 from chromatin extracts of neoplastic cells. Comp Biochem Physiol B Biochem Mol Biol. 2003; 134:425–33. [PubMed: 12628374]
31. Dayton TL, Gocheva V, Miller KM, Israelsen WJ, Bhutkar A, Clish CB, et al. Germline loss of PKM2 promotes metabolic distress and hepatocellular carcinoma. Genes Dev. 2016; 30:1020–33. [PubMed: 27125672]
32. Israelsen WJ, Dayton TL, Davidson SM, Fiske BP, Hosios AM, Bellinger G, et al. PKM2 isoform-specific deletion reveals a differential requirement for pyruvate kinase in tumor cells. Cell. 2013; 155:397–409. [PubMed: 24120138]
33. Staal JA, Lau LS, Zhang H, Ingram WJ, Hallahan AR, Northcott PA, et al. Proteomic profiling of high risk medulloblastoma reveals functional biology. Oncotarget. 2015; 6:14584–95. [PubMed: 25970789]
34. Kenney AM, Cole MD, Rowitch DH. Nmyc upregulation by sonic hedgehog signaling promotes proliferation in developing cerebellar granule neuron precursors. Development. 2003; 130:15–28. [PubMed: 12441288]
35. Garcia I, Crowther AJ, Gama V, Miller CR, Deshmukh M, Gershon TR. Bax deficiency prolongs cerebellar neurogenesis, accelerates medulloblastoma formation and paradoxically increases both malignancy and differentiation. Oncogene. 2013; 32:2304–14. [PubMed: 22710714]
36. Li B, Dewey CN. RSEM: accurate transcript quantification from RNA-Seq data with or without a reference genome. BMC Bioinformatics. 2011; 12:323. [PubMed: 21816040]
37. Dobin A, Davis CA, Schlesinger F, Drenkow J, Zaleski C, Jha S, et al. STAR: Ultrafast universal RNA-seq aligner. Bioinformatics. 2013; 29:15–21. [PubMed: 23104886]
38. Rubin LL, de Sauvage FJ. Targeting the Hedgehog pathway in cancer. Nat Rev Drug Discov. 2006; 5:1026–33. [PubMed: 17139287]
39. Salani B, Ravera S, Amaro A, Salis A, Passalacqua M, Millo E, et al. IGF1 regulates PKM2 function through Akt phosphorylation. Cell Cycle. 2015; 14:1559–67. [PubMed: 25790097]
40. Iqbal MA, Siddiqui FA, Gupta V, Chattopadhyay S, Gopinath P, Kumar B, et al. Insulin enhances metabolic capacities of cancer cells by dual regulation of glycolytic enzyme pyruvate kinase M2. Mol Cancer. 2013; 12:72–83. [PubMed: 23837608]

41. Dudek H, Datta SR, Franke TF, Segal RA, Kaplan DR, Greenberg ME. Regulation of neuronal survival by the serine-threonine protein kinase Akt. Science. 1997; 275:661–5. [PubMed: 9005851]
42. Helms AW, Abney AL, Ben-Arie N, Zoghbi HY, Johnson JE. Autoregulation and multiple enhancers control Math1 expression in the developing nervous system. Development. 2000; 127:1185–96. [PubMed: 10683172]
43. Machold R, Fishell G. Math1 is expressed in temporally discrete pools of cerebellar rhombic-lip neural progenitors. Neuron. 2005; 48:17–24. [PubMed: 16202705]
44. Goyal MS, Hawrylycz M, Miller JA, Snyder AZ, Raichle ME. Aerobic glycolysis in the human brain is associated with development and neotenous gene expression. Cell Metab. 2014; 19:49–57. [PubMed: 24411938]
45. Lunt SY, Muralidhar V, Hosios AM, Israelsen WJ, Gui DY, Newhouse L, et al. Pyruvate Kinase Isoform Expression Alters Nucleotide Synthesis to Impact Cell Proliferation. Mol Cell. 2015; 57:95–107. [PubMed: 25482511]
46. Johnson RL, Grenier JK, Scott MP. Patched Overexpression Alters Wing Disc Size and Pattern: Transcriptional and Post-Transcriptional Effects on Hedgehog Targets. Development. 1995; 121:4161–70. [PubMed: 8575316]
47. Goodrich LV, Jung D, Higgins KM, Scott MP. Overexpression of ptc1 inhibits induction of Shh target genes and prevents normal patterning in the neural tube. Dev Biol. 1999; 211:323–34. [PubMed: 10395791]
48. Eigenbrodt R, Reinacher M, Scheefers-Borchel U, Scheefers H, Friss R. Double role for pyruvate kinase type M2 in the expansion of phosphometabolite pools found in tumor cells. Crit Rev Oncog. 1992; 3:91–115. [PubMed: 1532331]
49. Tech K, Deshmukh M, Gershon TR. Adaptations of energy metabolism during cerebellar neurogenesis are co-opted in medulloblastoma. Cancer Lett. 2014; 356:268–72. [PubMed: 24569090]
50. Hosios AM, Hecht VC, Danai LV, Johnson MO, Rathmell JC, Steinhauser ML, et al. Amino Acids Rather than Glucose Account for the Majority of Cell Mass in Proliferating Mammalian Cells. Dev Cell. 2016; 36:540–9. [PubMed: 26954548]
51. Vander Heiden MG, Locasale JW, Swanson KD, Sharfi H, Heffron GJ, Amador-Noguez D, et al. Evidence for an alternative glycolytic pathway in rapidly proliferating cells. Science. 2010; 329:1492–9. [PubMed: 20847263]
52. Hitosugi T, Zhou L, Elf S, Fan J, Kang H-B, Seo JH, et al. Phosphoglycerate Mutase 1 Coordinates Glycolysis and Biosynthesis to Promote Tumor Growth. Cancer Cell. 2012; 22:585–600. [PubMed: 23153533]
53. Morris LGT, Chan TA. Therapeutic targeting of tumor suppressor genes. Cancer. 2015; 121:1357–68. [PubMed: 25557041]
54. Liu Y, Hu X, Han C, Wang L, Zhang X, He X, et al. Targeting tumor suppressor genes for cancer therapy. BioEssays. 2015; 37:1277–86. [PubMed: 26445307]
55. Tikunov AP, Johnson CB, Lee H, Stoskopf MK, Macdonald JM. Metabolomic investigations of American oysters using 1H-NMR spectroscopy. Mar Drugs. 2010; 8:2578–96. [PubMed: 21116407]
56. Millard P, Letisse F, Sokol S, Portais JC. IsoCor: Correcting MS data in isotope labeling experiments. Bioinformatics. 2012; 28:1294–6. [PubMed: 22419781]
57. Morin RD, Bainbridge M, Fejes A, Hirst M, Krzywinski M, Pugh TJ, et al. Profiling the HeLa S3 transcriptome using randomly primed cDNA and massively parallel short-read sequencing. Biotechniques. 2008; 45:81–94. [PubMed: 18611170]
58. Li H, Durbin R. Fast and accurate short read alignment with Burrows-Wheeler transform. Bioinformatics. 2009; 25:1754–60. [PubMed: 19451168]

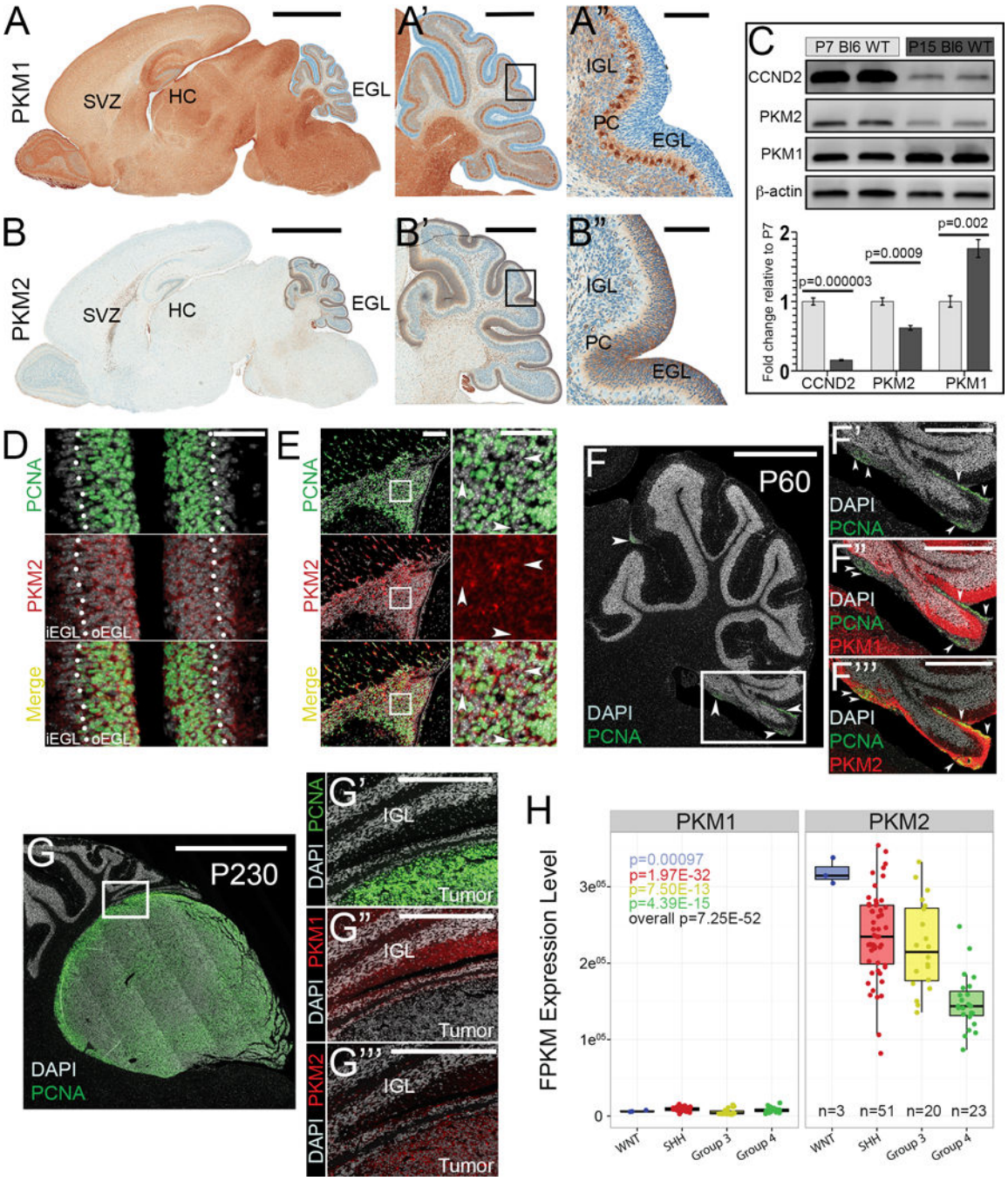

Figure 1. PKM1 and PKM2 correspond to differentiation state

IHC (brown) shows (A–A″) PKM1 in differentiated neurons throughout the brain and (B–B″) PKM2 in neural progenitors of the SVZ, HC, and EGL. (C) Western blot of CCND2, PKM2, and PKM1 in whole cerebellum lysates harvested at the indicated age, normalized to β-actin. PKM2 decreases from P7 (n=4) to P15 (n=4), while PKM1 increases. Graph presents mean±s.e.m. Immunofluorescence shows PKM2 in (D) the PCNA+ oEGL and the PCNA− iEGL of in P7 wildtype mice and (E) PKM2 in PCNA+ and PCNA− (arrowheads) SVZ progenitors. (F) Premalignant lesions in P60 *ND2:SmoA1* mice identified by PCNA,

are PKM2+ and PKM1−. (G) PKM2 and PCNA are expressed in a *ND2:SmoA1* medulloblastoma; adjacent normal tissue expresses PKM1. (H) RNA-seq shows preferential expression of PKM2 in all human medulloblastoma subgroups. *P*-values determined by Student's *t*-tests. High magnification of boxed areas shown on the right. PC=Purkinje cell layer; ML=molecular layer; FPKM=Fragments Per Kilobase of transcript per Million mapped reads. Scale bars: 2 mm (A,B,G); 600 μm (A′,B′); 100 μm (A″,B″,E); 50 μm (D,E inset); 1 mm (F); 500 μm (F′–F‴); 300 μm (G′–G‴).

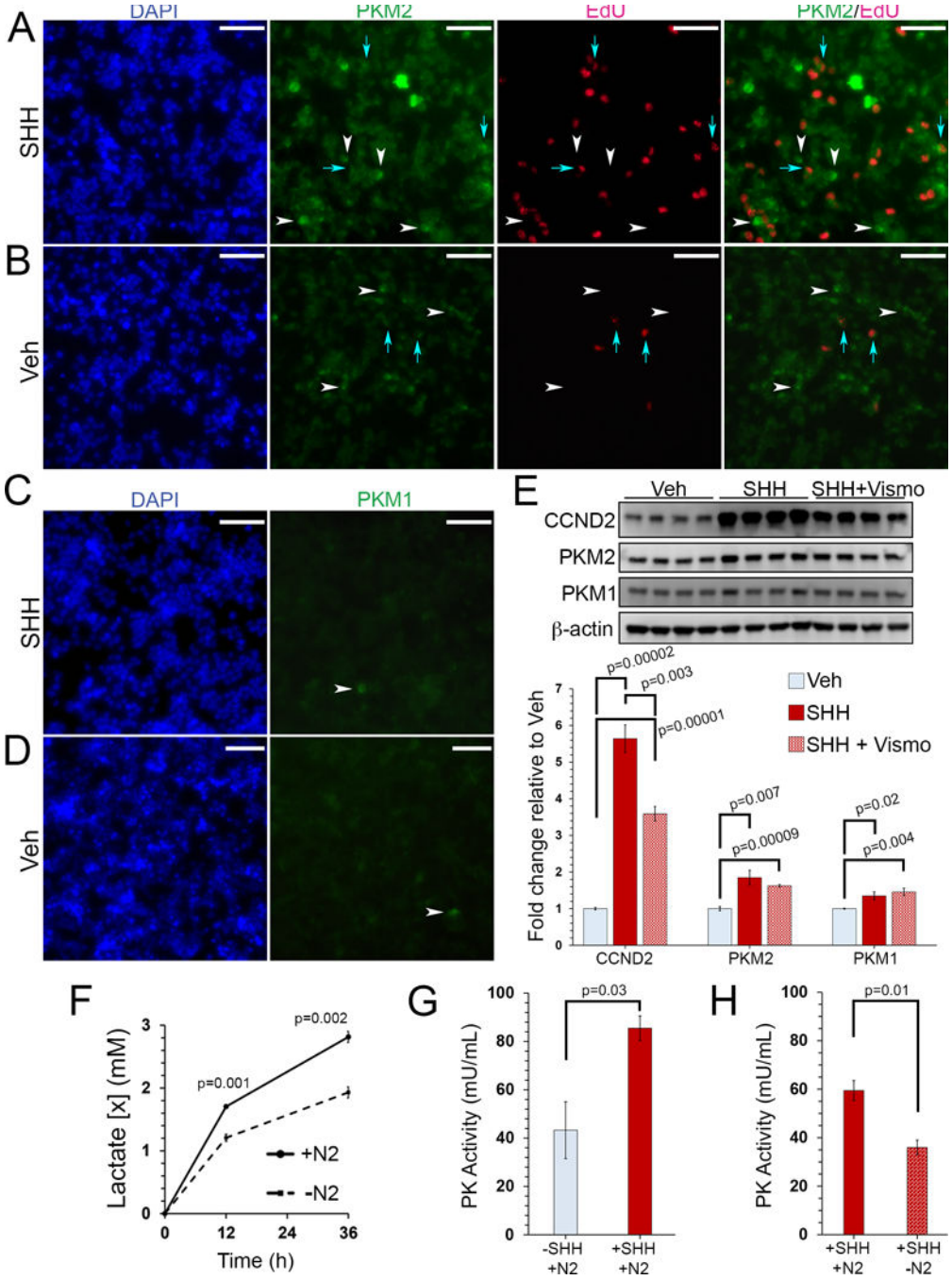

Figure 2. Growth factor signaling regulates PKM expression and activity

(A,B) PKM2 immunofluorescence on explanted CGNPs exposed to EdU for 1h, +/− SHH. (C,D) Rare cells within CGNP explants expressed PKM1 (arrowheads) in both SHH-treated and vehicle-treated wells. (E) Quantitative Western blot of CCND2, PKM2, and PKM1 in cell cultures, normalized to β-actin (n=4/condition). (F) N2-deprived CGNPs produce less lactate detected by enzymatic assay (n=3/condition). (G,H) CGNP PK activity increases with combined SHH and N2 supplementation (n=3/condition). Graphs present mean±s.e.m. *P*-values determined by Student's *t*-tests. Scale bars: 50μm.

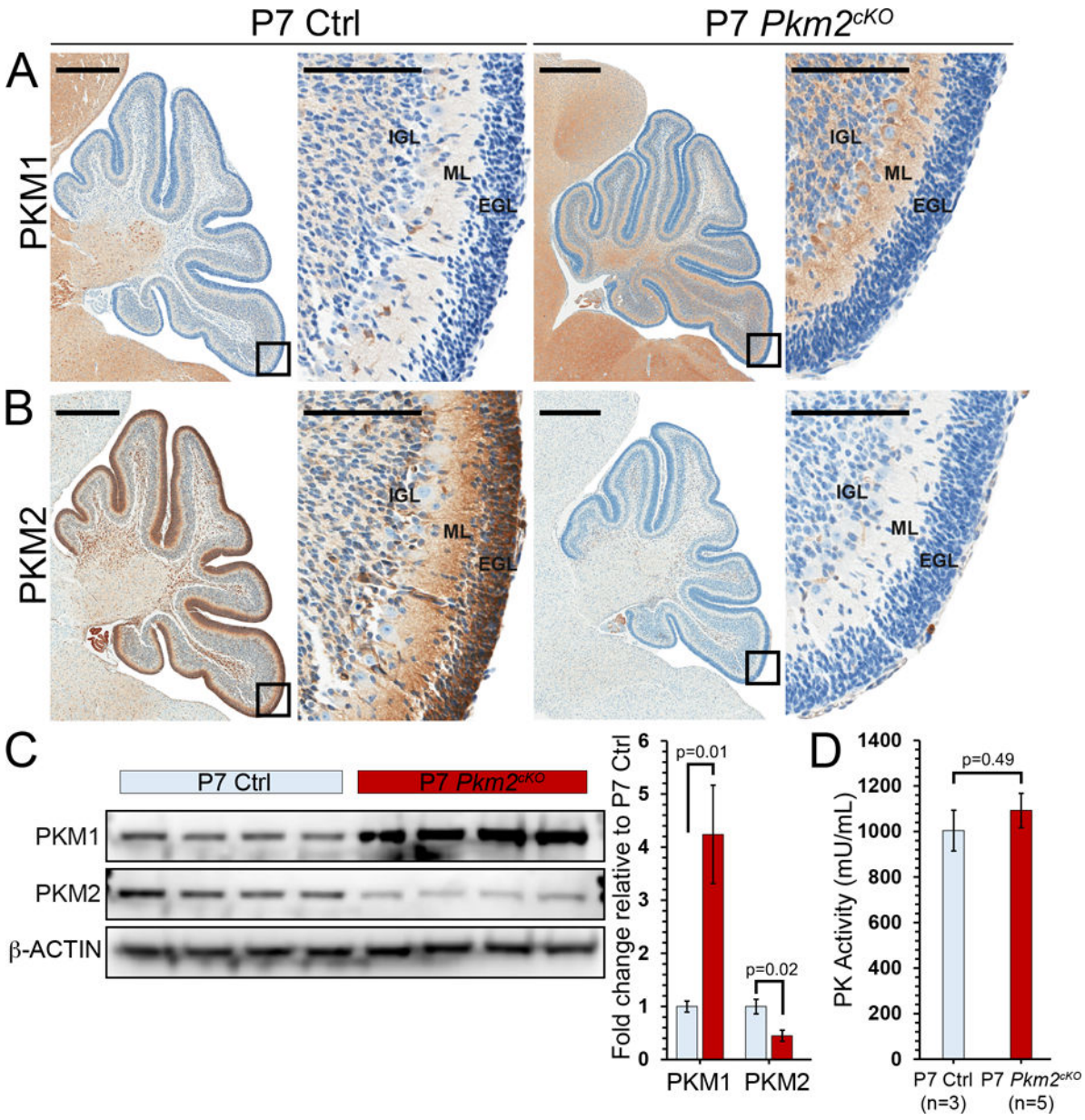

Figure 3. *Pkm2* deletion blocks all PKM expression in CGNPs

(A,B) IHC shows PKM1 and PKM2 in representative sagittal cerebellar sections from P7 Ctrl and *Pkm2*^{cKO} mice. *Pkm2* deletion does not induce compensatory PKM1 expression in the EGL. High magnification of boxed area is shown on the right. (C) Quantitative Western blot normalized to β-actin in whole P7 cerebellum lysates demonstrates decreased PKM2 and increased PKM1 (n=4/condition). (D) PK activity in whole P7 cerebellum lysates is similar between genotypes. Graphs present mean±s.e.m. *P*-values determined by Student's *t*-tests. Scale bars: 500μm; 100μm (insets).

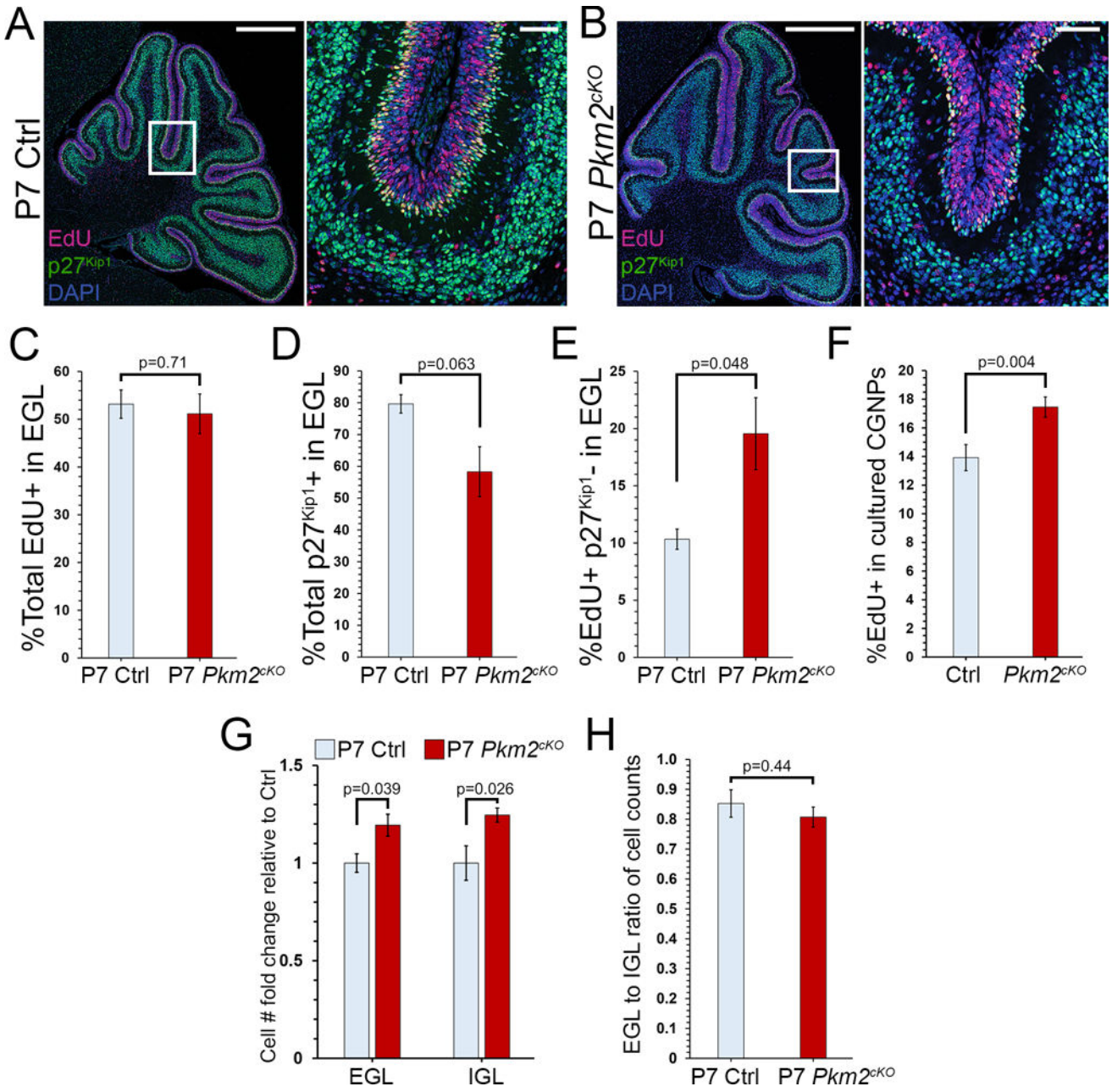

Figure 4. *Pkm2* deletion increases CGNP proliferation

(A,B) Representative confocal images of P7 Ctrl and *Pkm2*^{cKO} cerebellar sections labeled for the p27^{Kip1} and for EdU, 24h after EdU injection (n=3/condition). High magnifications of boxed areas are shown on the right. (C,D) Quantification of EdU+ cells and p27^{Kip1}+ cells in the EGL. (E) The p27^{Kip1}− fraction of the EdU+ population is significantly larger in the *Pkm2*^{cKO} EGL, indicating increased cell cycle re-entry. (F) Comparison EdU incorporation by CGNPs of indicated genotype, cultured with SHH and exposed to EdU for 1h. (G,H) Analysis of midsagittal cerebellar sections shows increased EGL and IGL populations in *Pkm2*^{cKO} mice (n=5) versus controls (n=4), with preserved EGL:IGL ratio.

Graphs present mean±s.e.m. *P*-values determined by Student's *t*-tests. Scale bars: 500μm; 50μm (insets).

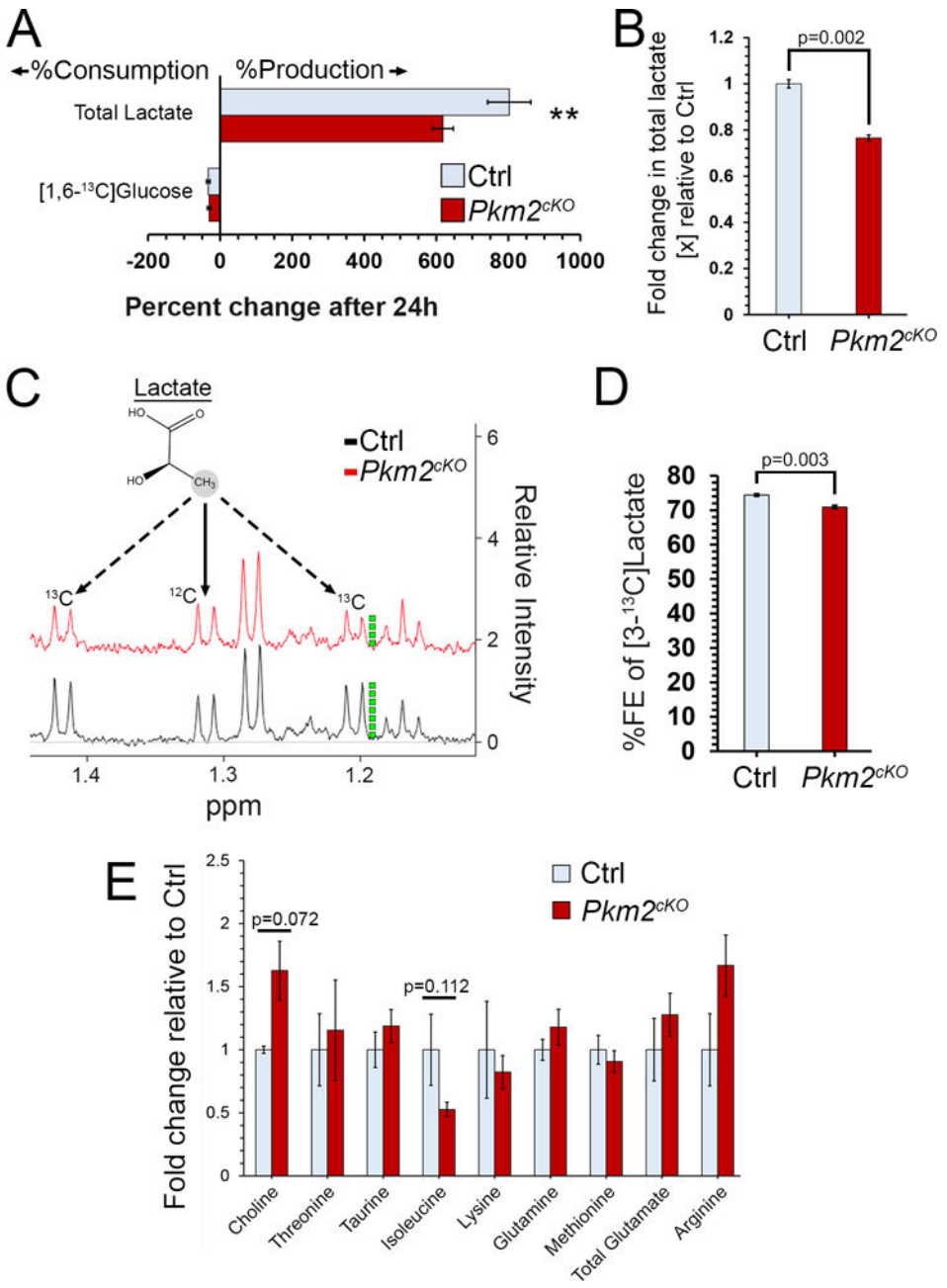

Figure 5. *Pkm2* deletion reduces lactate production

(A) ^{1}H NMR analysis of media sampled after 24h of culture demonstrates decreased lactate in *Pkm2*^{cKO} wells (n=4) compared to controls (n=3) (**p=0.029). (B) Comparison of media lactate between genotypes, measured by enzymatic assay. (C) Representative ^{1}H NMR spectra of Ctrl and *Pkm2*^{cKO} 24h media demonstrate the peaks representing [3-^{13}C] lactate (dashed line) and unlabeled lactate (solid line). (D) Quantification of ^{13}C-enriched fraction of lactate, from samples in (A). (E) LC-MS analysis of indicated metabolites in CGNP extracts, comparing genotypes. Graphs present mean±s.e.m. *P*-values determined by Student's *t*-tests. FE=fractional enrichment.

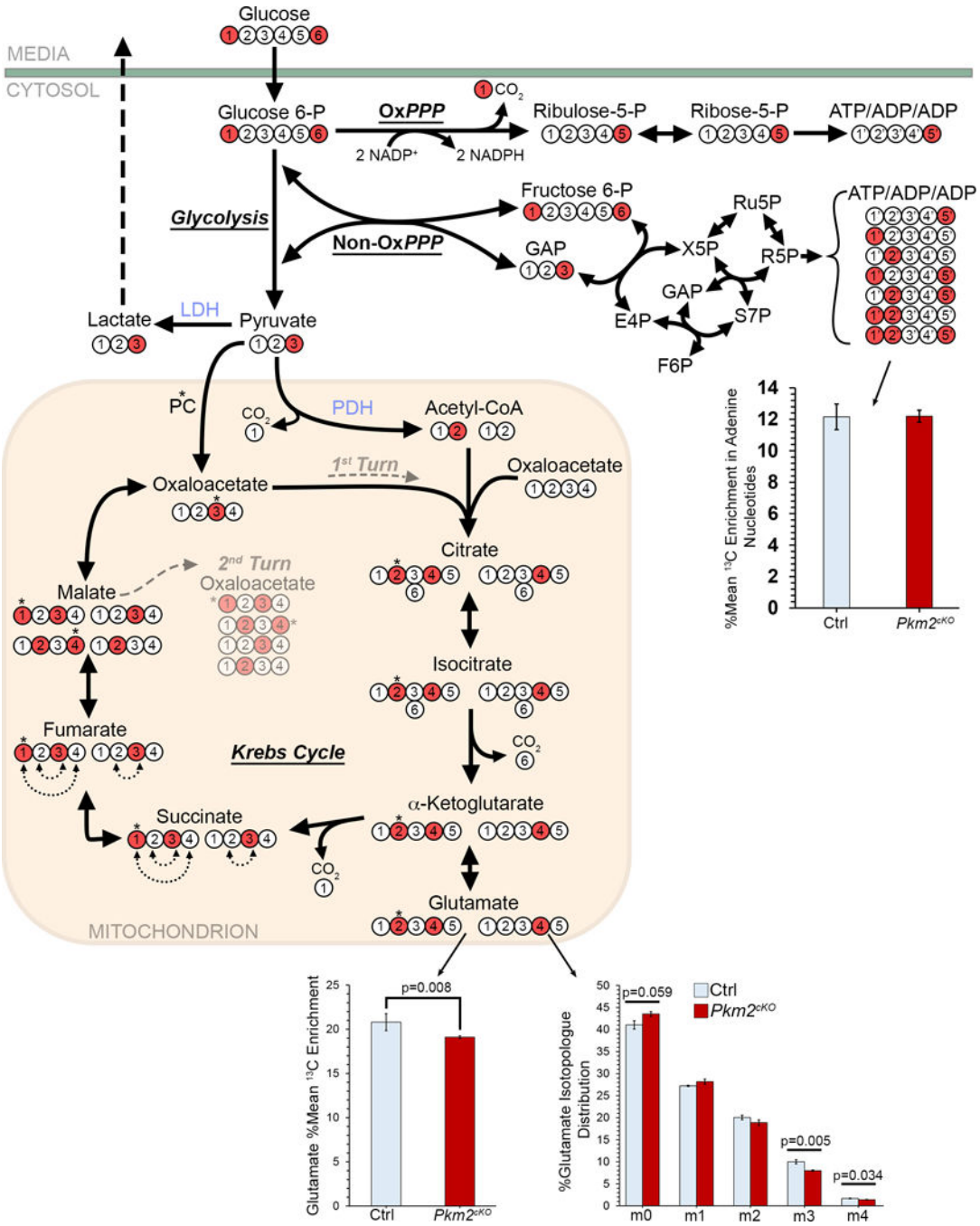

Figure 6. *Pkm2*-deleted CGNPs show altered glutamate progression through the Krebs cycle but comparable PPP flux

Comparison between SHH-treated CGNPs of indicated genotypes cultured for 24h with [1,6-^{13}C] glucose, showing ^{13}C labeling of ribose-labeled adenine nucleotides, and glutamate (mean±s.e.m). The diagram is provided to show how ^{13}C glucose carbons accumulate in ribose and glutamate. *P*-values determined by Student's *t*-tests. Ox*PPP*=oxidative phase of pentose phosphate pathway; Non-Ox*PPP*=non-oxidative phase of pentose phosphate pathway; GAP=glyceraldehyde-3-phosphate; X5P=xylulose-5-phosphate; E4P=erythrose-4-phosphate; F6P=fructose-6-phosphate; S7P=Sedoheptulose-7-phosphate;

R5P=ribose-5-phosphate; Ru5P=ribulose-5-phosphate; LDH=lactate dehydrogenase; PDH=pyruvate dehydrogenase; PC=pyruvate carboxylase.

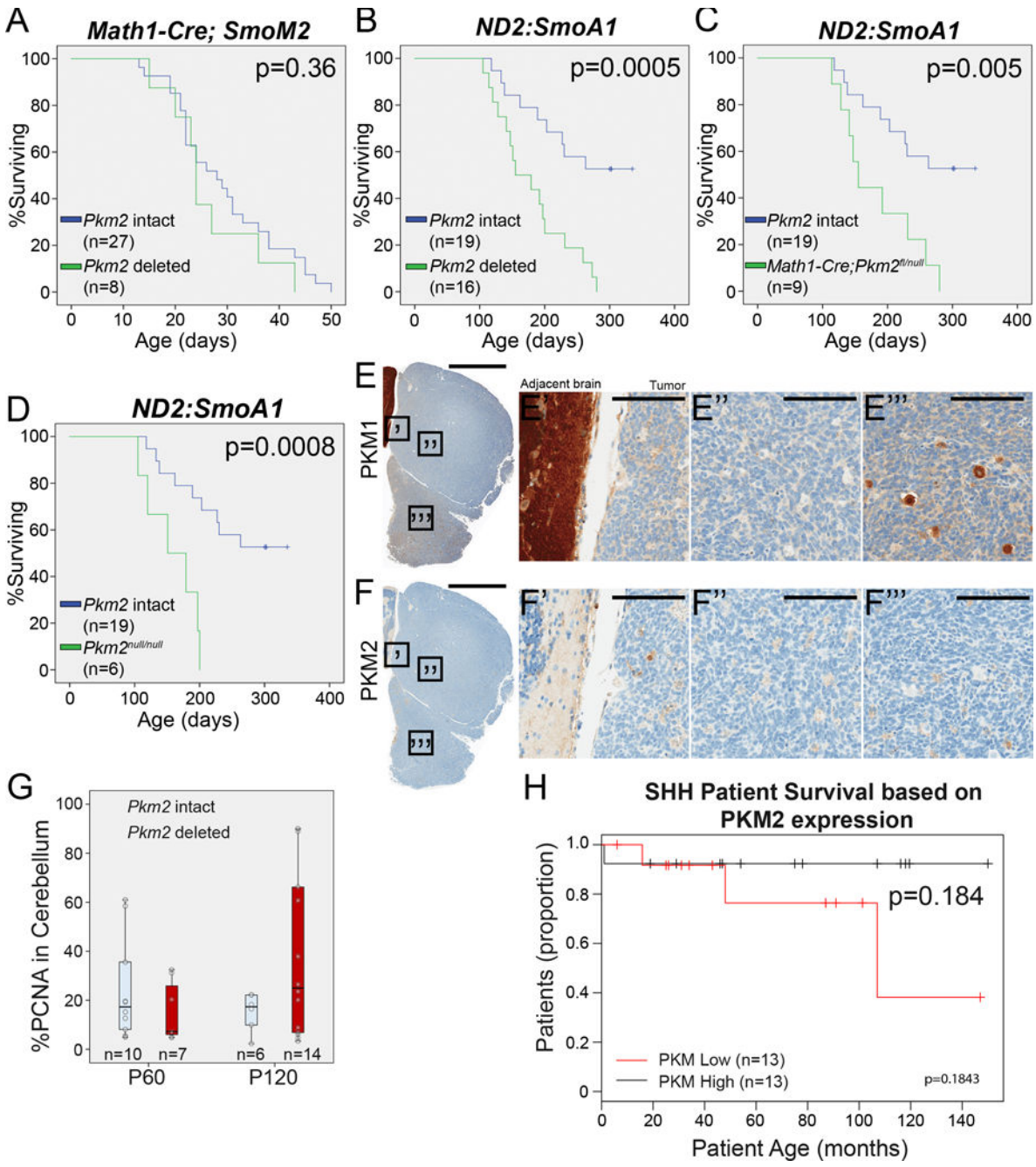

Figure 7. *Pkm2* deletion accelerates medulloblastoma tumorigenesis

(A–D) Kaplan-Meier curves demonstrate the effect of *Pkm2* deletion on survival in (A) the rapidly progressive *Math1-Cre;SmoM2* model and (B) the slow-growing *ND2:SmoA1* model, including (C) *ND2:SmoA1* mice with (C) conditional or (D) global *Pkm2* deletion. (E,F) A representative P147 *Pkm2*-deleted *ND2:SmoA1* medulloblastoma shows (E–E‴) PKM1 (brown) in normal brain and (F–F‴) absence of PKM2 (brown). (G) Comparison of premalignant lesions at P60 and P120 between genotypes. The proportion of PCNA+/total cells in the cerebellum increases over time in the *Pkm2*-deleted genotypes. (H) Kaplan-Meier curve demonstrates a trend toward shorter survival in SHH medulloblastoma patients

with low PKM2 expression. *P*-values determined by log-rank test (A–D), cox proportional hazard model (H), and by Student's *t*-test (G). Scale bars: 2mm (E,F); 100μm (E′-E‴,F′-F‴).